Available online at www.sciencedirect.com
ScienceDirect
Optics Communications 276 (2007) 31–36
OPTICS COMMUNICATIONS
www.elsevier.com/locate/optcom

High-resolution through-focus metric with two-pitch grating target

Deh-Ming Shyu [a,*], Mao-Hong Lu [a], Chun-Hung Ko [b]

[a] Department of Photonics and Institute of Electro-Optical Engineering, National Chiao Tung University, 1001 Ta Hsueh Road, Hsinchu 300, Taiwan, ROC
[b] Industrial Technology Research Institute, 321 Kuang Fu Road 2, Hsinchu 300, Taiwan, ROC

Received 20 October 2006; received in revised form 12 February 2007; accepted 4 April 2007

Abstract

Through-focus focus-metric is a method that is used to analyze images on a fixed plane with the help of focus-metric values when the target moves through the focus. In this study, an optical microscope having a magnification of 250× is constructed. A two-pitch grating target is imaged on a CCD detector and through-focus image data are measured. In addition, the optical field on the CCD detector is simulated using the boundary element method and physical optics propagation. By comparing the measured focus-metric signatures with the simulated signatures, information regarding the linewidth is obtained. The results show that the through-focus focus-metric method is a very sensitive method that can be used for measuring parameters such as the linewidth. Thus, a nanoscale resolution can be achieved.

1. Introduction

Advancements in the semiconductor industry have given rise to the requirement for reliable critical dimension (CD) metrology techniques. According to a developmental report of semiconductor technology presented in ITRS 2005 (International Technology Roadmap for Semiconductor), a physical gate length of 32 nm requires a gate CD control (accuracy) of below 3.3 nm and a CD metrology tool precision of 1.77 nm. An optical microscope is a conventionally used metrological tool that uses an imaging method at the best focal plane for detecting the CD. However, if the CD is substantially smaller than the wavelength used in the optical microscope, it is difficult to measure the CD correctly by using the imaging method because of the diffraction limit [1,2].

The technique of scatterometry [3–5] has been proposed to measure the CD by using a grating target. Light scattered by a grating is very sensitive to changes in the CD corresponding to the feature size of the grating. However, if this phenomenon is to be simulated with the rigorous coupled-wave algorithm (RCWA) [6–8], a grating with a large number of pitches is required for satisfying the condition of this algorithm. Another method is the through-focus focus-metric method [9–11] using an optical microscope. When the target moves through the focus, a CCD detector measures the image data. The through-focus image data are analyzed by the focus metric (FM) [12] that provides the relation between the intensity distribution and the structure parameters of the grating target. This measurement system is easy to execute and can be analyzed by the focus metric. In the through-focus focus-metric method, RCWA and ray tracing are combined to simulate through-focus images. Because the RCWA is used, a large number of pitches is required, for which the dimension of the grating target must be sufficiently large. However, the dimension of the fabricated bar-in-bar or box-in-box structure is only approximately several micrometers. In this case, the grating target, which contains a small number of pitches, cannot satisfy the condition of RCWA. Therefore, instead of RCWA, another method must be used to simulate the through-focus images for use in CD metrology.

In this study, we simulate and analyze the optical microscope system for a two-pitch grating by using the boundary

* Corresponding author. Tel.: +886 968760809; fax: +886 3 5722383.
E-mail addresses: sidney.eo89g@nctu.edu.tw (D.-M. Shyu), mhlu@cc.nctu.edu.tw (M.-H. Lu), kavanko@itri.org.tw (C.-H. Ko).

0030-4018/$ - see front matter © 2007 Elsevier B.V. All rights reserved.
doi:10.1016/j.optcom.2007.04.001

element method (BEM) [13–16] in the near field and physical optics propagation in the far field. Because the BEM is a boundary-type methods that is based on the integral equation method, it can reduce the matrix dimension significantly in comparison with other domain-type methods such as the finite element method (FEM) [17] or the finite-difference time-domain method (FDTD) [18,19]. In the far field, the commercial optics software ASAP is used to calculate the intensity distribution. In ASAP, a Gaussian beam superposition algorithm models an arbitrary optical fields as a coherent sum of fundamental Gaussian beams. Furthermore, each Gaussian beam is represented by a set of real rays describing the coherence, polarization, amplitude, and phase of the Gaussian beam. These rays can be traced through the optical microscope system. It is possible to superpose the ray trace information from each Gaussian beam in order to recreate the optical field at any position in space. In this case, when the target moves through the focus, the field reflected from the target in the near field is calculated using the BEM. Then, the images on the plane that is located at the best focus for a given object distance are calculated by physical optics propagation. A series of the images is taken and analyzed by the focus-metric method. In this study, the relation between the focus-metric value and the parameters of the grating, such as the linewidth, pitch, etc., has been determined. According to this analysis and our experimental results, a change of several nanometers in the CD can be resolved.

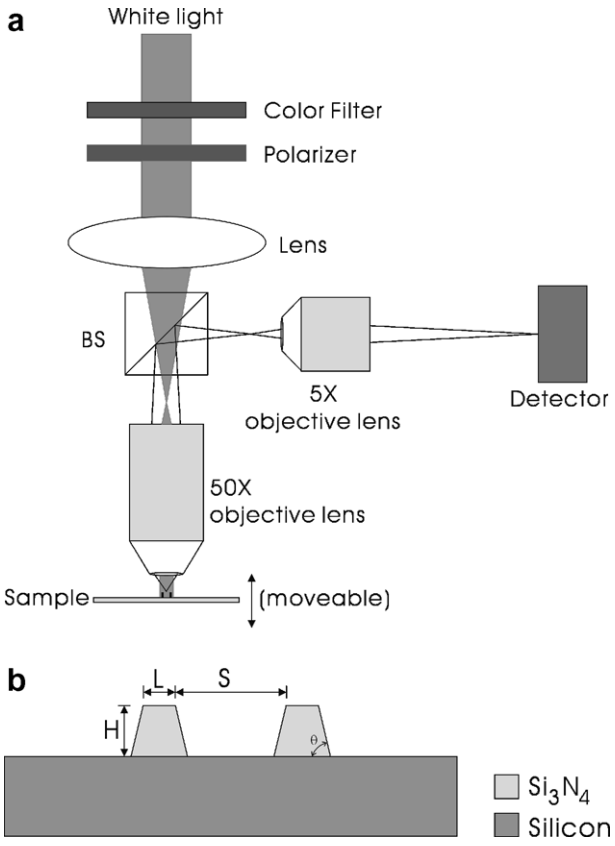

Fig. 1. Schematic diagrams of optical microscope (a) and the grating structure (b).

2. Analysis methods

A schematic diagram of the optical microscope and the two-pitch grating target is shown in Fig. 1. Parameters L, S, and H denote the linewidth, space, and thickness of the grating, respectively. The pitch of the grating is the summation of L and S. In this system, s-polarized light having a bandwidth from 480 nm to 550 nm is normally incident on the grating. At various object distances, the target is imaged on the CCD detector by the microscope. The two-pitch grating target is made of silicon (Si) and silicon nitride (Si_3N_4), as shown in Fig. 1b. We use two algorithms to simulate the optical system with the two-pitch grating target. One algorithm is the BEM that is used to calculate the field reflected from the two-pitch grating in the near-field region. The other algorithm is physical optics propagation that is used to calculate the image in the region from the near field to the CCD detector through the optical microscope.

For the near-field calculation of the field reflected from the two-pitch grating target, the space is divided into four homogeneous subregions S_1 to S_4 that are separated by three boundaries Γ_1 to Γ_3, as shown in Fig. 2. The refractive index in subregion S_i is denoted by n_i, $i = 1,2,3,4$. Because n_1 and n_2 correspond to the refractive index of free space, the values of n_1 and n_2 are taken as unity. Subregions S_3 and S_4 correspond to Si_3N_4 and the Si substrate,

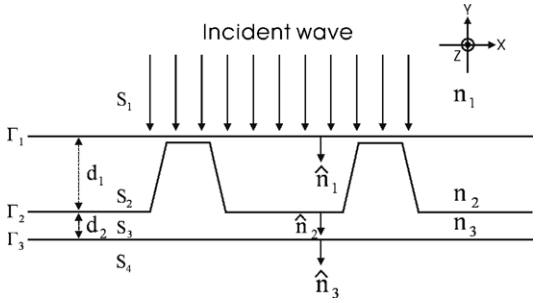

Fig. 2. The grating structure with three boundaries.

respectively. A plane wave with unit amplitude is normally incident on boundary Γ_1, which is a dummy boundary that has no effect on the optical field because the refractive indices on the both sides are the equal. The field reflected from the two-pitch grating can be calculated in subregion S_1 as follows. By applying Green's theorem to Maxwell's equations and taking into account radiation and the boundary conditions, the regional integral equations can be expressed as [20]

$$\phi_1^t(r_1) + \int_{\Gamma_1} \left[\phi_{\Gamma_1}(r'_{\Gamma_1})\hat{n}_1 \cdot \nabla G_1(r_1, r'_{\Gamma_1}) - p_1 G_1(r_1, r'_{\Gamma_1})\psi_{\Gamma_1}(r'_{\Gamma_1})\right] d\ell' = \phi^{inc}(r_1), \quad r_1 \in S_1, \tag{1}$$

$$\phi_i^{\mathrm{t}}(r_i) - \sum_{m=1}^{2} \int_{\Gamma_{(i-2)+m}} \Big[\phi_{\Gamma_{(i-2)+m}}(r'_{\Gamma(i-2)+m})\hat{n}_{(i-2)+m} \cdot \nabla G_i(r_i, r'_{\Gamma_{(i-2)+m}}) - p_i G_i(r_i, r'_{\Gamma_{(i-2)+m}}) \psi_{\Gamma_{(i-2)+m}}(r'_{\Gamma_{(i-2)+m}}) \Big] \mathrm{d}\ell' = 0, \quad r_i \in S_i, \ i = 2, 3, \tag{2}$$

$$\phi_4^{\mathrm{t}}(r_4) - \int_{\Gamma_3} \Big[\phi_{\Gamma_3}(r'_{\Gamma_3})\hat{n}_3 \cdot \nabla G_4(r_4, r'_{\Gamma_3}) - p_4 G_4(r_4, r'_{\Gamma_3}) \psi'_{\Gamma_3} \Big] \mathrm{d}\ell' = 0 \quad r_4 \in S_4, \tag{3}$$

where

$$G_i\left(r_i, r'_{\Gamma_{(i-2)+m}}\right) = \frac{-j}{4} H_0^{(2)}\left(k_i | r_i - r'_{\Gamma_{(i-2)+m}} |\right) \quad i = 1, 2, 3, 4. \tag{4}$$

Here, $\phi = E_Z$ and $p_i = 1$ for the transverse electric (TE) mode, and $\phi = H_Z$ and $p_i = n_i^2$ for the transverse magnetic (TM) mode ($i = 1, 2, 3, 4$). ϕ^{t} and ϕ^{inc} are the total and incident field, respectively. G_i is the two-dimensional Green's function, and $H_0^{(2)}$ is the zero-order Hankel function of the second kind. Vectors r_i and $r'_{\Gamma_{(i-2)+m}}$ are the position vectors of the points in subregion S_i and on boundary Γ_m, respectively. In addition, the electromagnetic boundary conditions that must hold on boundary Γ (continuity of tangential electric field and magnetic field components) are given by

$$\phi_{\Gamma_i}(r_{\Gamma_i}) = \phi_i^{\mathrm{t}}(r_{\Gamma_i}) = \phi_{i+1}^{\mathrm{t}}(r_{\Gamma_i}), \tag{5}$$

$$\psi_{\Gamma_i}(r_{\Gamma_i}) = \left(\frac{1}{p_i}\right)\hat{n}_i \cdot \nabla \phi_i^{\mathrm{t}}(r_{\Gamma_i}) = \left(\frac{1}{p_{i+1}}\right)\hat{n}_i \cdot \nabla \phi_{i+1}^{\mathrm{t}}(r_{\Gamma_i}), \quad i = 1, 2, 3, 4. \tag{6}$$

In this case, the boundary integral equations can be divided by using a number of nodes on the boundaries Γ_1 to Γ_4, and the fields at these nodes are determined by using the BEM with quadratic elements. From these values, at any point on boundary Γ_i, field values ϕ_{Γ_i} and their derivatives ψ_{Γ_i} can be calculated by quadratic interpolation. After the boundary values are known, the total field at any point r_i in subregion S_i can be determined by Eqs. (1)–(3). The details of the through-focus calculation are described in [21].

We calculate the intensity distribution of the field reflected from the two-pitch grating. The refractive indices for different wavelengths are shown in Table 1, and the incident wavelength is 530 nm. The values of L, S, H and θ are 0.7 μm, 3.0 μm, 50 nm, and 90°, respectively. The values of d_1 and d_2 are 55 nm and 0 nm, respectively. The simulation result for the TE mode is shown in Fig. 3. The intensity distribution of the reflective field is caused by light scattered from the two-pitch grating. The amplitude and phase of the optical field on boundary Γ_1 are used as the wavefront of the object field for the optical microscope. Images are taken by the CCD detector using a magnification of 250×; this magnification is obtained from the combination of 50× and 5× objective lenses.

The parameters of the 50× and 5× objective lenses used in both the simulation and the experiment are shown in Table 2 and Table 3, respectively. The numerical apertures (NAs) of the 50× and 5× objective lenses are 0.55 and 0.1, respectively. The working distance is 13.0 mm and the image distance is 160.0 mm. The wavefront of the object field for the optical microscope is obtained from boundary Γ_1 and is imaged on the CCD detector by the physical optics propagation. In this case, the intensity distributions on boundary Γ_1 and on the CCD detector are calculated from the amplitude and phase, as shown in Fig. 4.

3. Experimental arrangement and theoretical simulation

The through-focus focus-metric method is used as a metrology technique to determine the geometric parameters

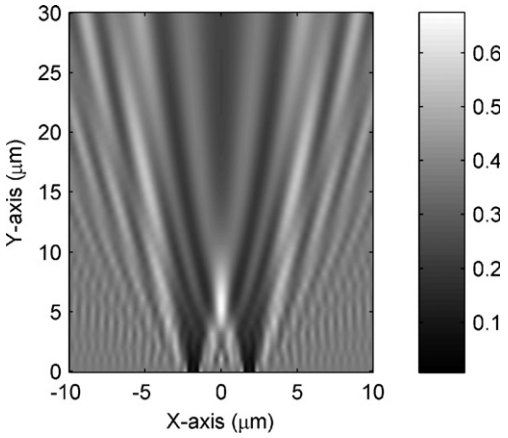

Fig. 3. The intensity distribution of two-pitch grating for the reflection field. The two-pitch grating is located at $y = 0.0$ μm.

Table 1
The refractive index of material at the wavelength from 480 nm to 550 nm

	Si	Si_3N_4
480 nm	4.422–0.0871i	2.0694
490 nm	4.353–0.0781i	2.0650
500 nm	4.296–0.0703i	2.0609
510 nm	4.246–0.0640i	2.0570
520 nm	4.195–0.0581i	2.0533
530 nm	4.149–0.0527i	2.0498
540 nm	4.108–0.0473i	2.0464
550 nm	4.073–0.0406i	2.0433

Table 2
The parameters of the 50× objective lens

Number	Radius	Conic	Thickness (mm)	Refractive index	Half width (mm)
1 (object)			13.0		
2	−68.629	17.672	20.0	2.0	8.25
3	−29.287	−0.172	12.0		14.50
4	84.237	0.531	20.0	2.0	18.21
5	−123.541	−2.336	26.0		18.01
6	27.622	−0.122	20.0	2.0	12.69
7	61.422	19.011	6.0		6.88
8	−16.386	−1.279	15.0	2.0	3.92
9	8.484	−1.291	178.8		2.06

Table 3
The parameters of the 5× objective lens

Number	Radius	Conic	Thickness (mm)	Refractive index	Half width (mm)
1			50.0		
2	26.689		10.0	2.0	5.34
3	673.267		2.6		4.64
4	53.350	−5.799	10.0	2.0	4.44
5	38.360	8.255	1.0		3.865
6	−222.480	401.682	10.0	2.0	3.858
7	93.418	66.783	160.0		3.905
8 (image)					

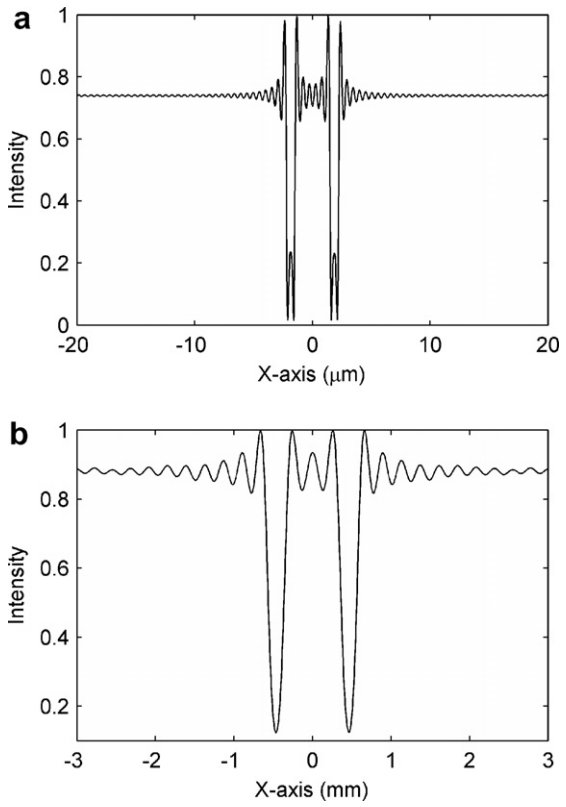

Fig. 4. The intensity distributions on the boundary Γ_1 (a) as the object of the optical microscope and on the image plane (b) with the magnification of 250×.

of the grating target by using the images of the target at different object distances. The experimental arrangement is illustrated in Fig. 5. White light is used as the light source. A color filter and polarizer is used to control the bandwidth and polarization of the input beam. In this experiment, only TE mode is considered, and the bandwidth of the beam is from 480 nm to 550 nm. The incident beam is normally incident on the surface of the two-pitch grating target. The target moves along the optical axis by a step motor, and a series of images are taken by a CCD detector that is located at the conjugate plane of target which is at the working distance of the optical microscope. The optical microscope is the combination of 50× and 5× objective lenses and the magnification is 250×. In this experiment, the designed values of L, S, H and θ are 0.7 μm, 3.0 μm, 50 nm, and 90°, respectively. The width of the grating along the z direction is 4.7 μm. However, it is observed that the real parameter values of the fabricated two-pitch grating are slightly different from the designed values. The sample is measured by transmission electron microscopy (TEM), as shown in Fig. 6. The measured values of L, H, θ, and d_2 are 671.3 nm, 49.7 nm, 52.63°, and 2.9 nm, respectively.

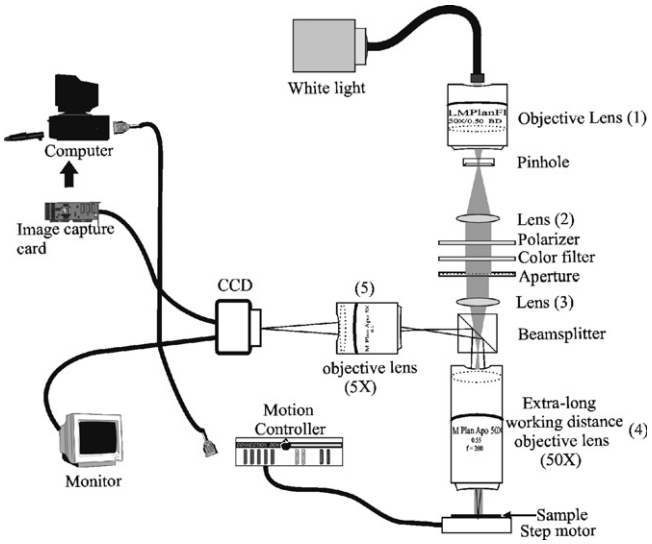

Fig. 5. Experimental arrangement.

In the simulation, the bandwidth of the incident beam which is from 480 nm to 550 nm should be considered. First, we calculate the intensity distributions of individual wavelengths from 480 nm to 550 nm with steps of 10 nm, as shown in Fig. 7a, and then take the weighted sum of them to obtain the intensity distribution over the bandwidth from 480 nm to 550 nm, as shown in Fig. 7b. After the summation, the fluctuation in the intensity distribution on the boundary of the grating becomes smoother. In our system, the object distance is variable. When the target is moving along the optical axis, the intensity distribution on the fixed image plane changes due to defocus. Fig. 8 shows the intensity distributions for defocuses of 0 μm,

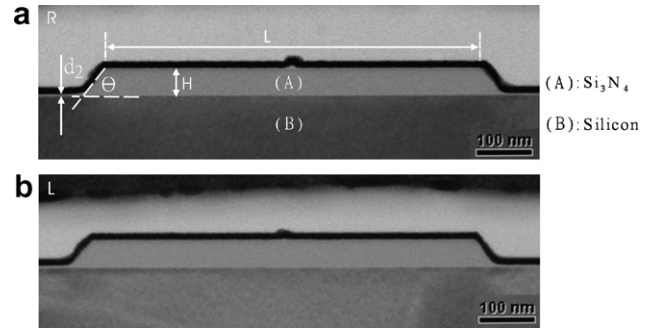

Fig. 6. The cross section of the sample measured with TEM. (a) is the right-side grating and (b) is the left-side grating. The values of L, H, θ and d_2 are 671.3 nm, 49.7 nm, 52.63° and 2.9 nm, respectively.

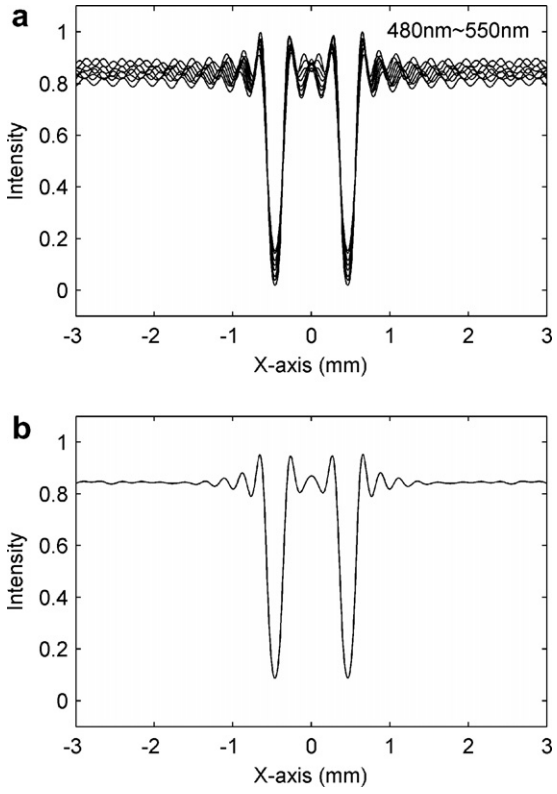

Fig. 7. The intensity distributions for different wavelengths are in (a) and the intensity distribution for the band-width from 480 nm to 550 nm is in (b).

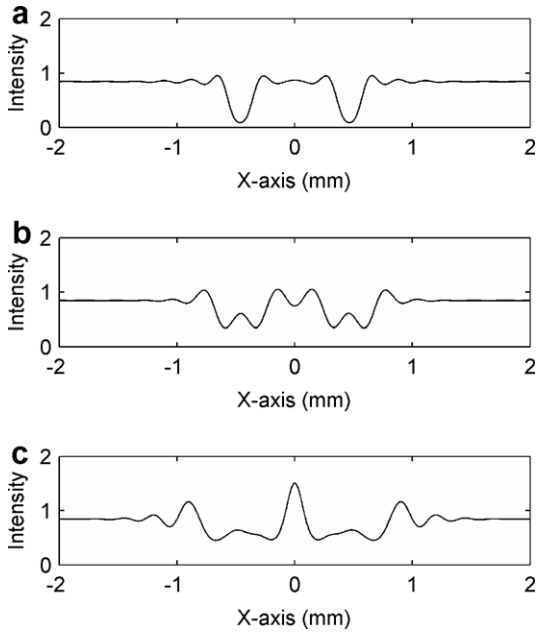

Fig. 8. The intensity distributions on the fixed image plane with band-with from 480 nm to 550 nm for defocuses 0 μm (a), 2.5 μm (b), and 5.0 μm (c).

2.5 μm, and 5.0 μm with the broadband incident beam. Information regarding the parameters of the two-pitch grating is contained in the intensity distribution for different defocuses. In order to analyze the intensity distribution, we use the focus-metric method of gradient energy. The gradient energy is defined as

$$\mathrm{FM}_{\mathrm{GE}} = \frac{1}{m}\sum_{i=1}^{m} |\nabla f(x_i)|^2, \tag{7}$$

where m denotes the total number of sampling points, ∇ is the gradient operator, and $f(x)$ is the function of the intensity distribution on the x axis. The calculation range of x in the intensity distribution is from -2 mm to $+2$ mm. Fig. 9 shows the focus-metric signature obtained by calculating the designed structure using the through-focus focus-metric method. The range of the defocus is from -15 μm to $+20$ μm, and the image plane is located at the conjugate plane where the defocus of target is zero and the gradient energy is at its peak. For different parameter of grating, the distribution of gradient energy is different, and it can be calculated by using the BEM and physical optics propagation.

4. Measurement and result

The two-pitch grating is measured by the 250× optical microscope with the through focus from -20 μm to $+20$ μm, and it is imaged on the CCD detector. The focus-metric values of the gradient energy are calculated from the through focuses of images. Then, the focus-metric signature of the gradient energy is obtained. Based on the real parameters measured by TEM, the focus-metric signature for the gradient energy is calculated by the BEM and physical optics propagation. The results of the measurement and the simulation are shown in Fig. 10. In this figure, the circles represent the values measured by the optical microscope, and the three lines correspond to the simulation results calculated by the BEM and physics optical propagation for three different values of L: 666 nm, 671 nm, and 676 nm. This shows that the algorithm used by combining the BEM and physics

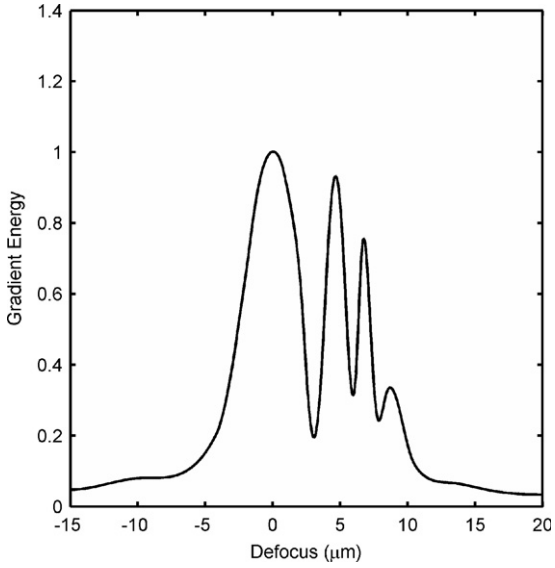

Fig. 9. The focus-metric signature for gradient energy.

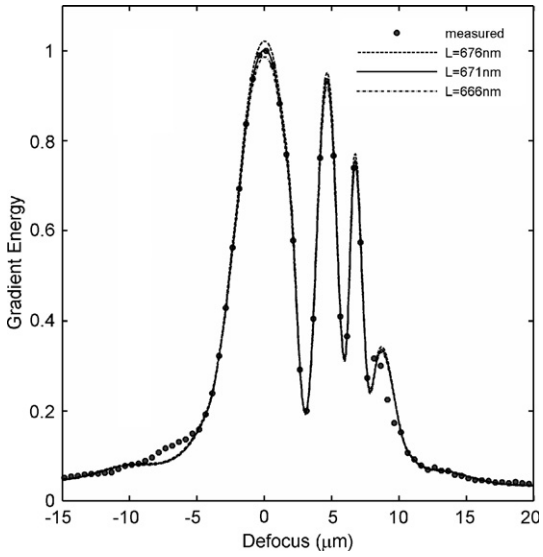

Fig. 10. The measured and simulated focus-metric signatures of the gradient energy.

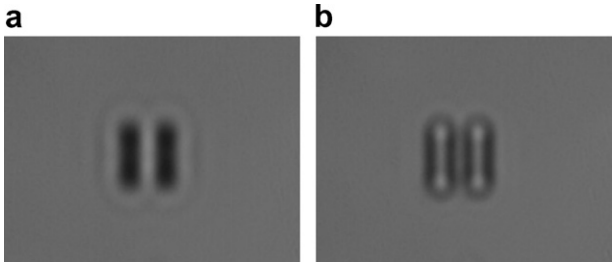

Fig. 11. The images for the defocus of 0 μm (a) and 4.5 μm (b). The phase difference between (a) and (b) is 180°.

optical propagation is suitable for performing the simulation of the through-focus focus-metric method. From Fig. 11, it can be seen that the phase difference between the images of the defocus at 0 μm and 4.5 μm is 180°. This result should be attributed to the Talbot effect [22].

5. Conclusion

In this study, a method that combines the algorithm of BEM and physical optics propagation is used to calculate the through-focus images. Furthermore, the focus-metric of gradient energy is used for analyzing the images. In the experiment, a two-pitch grating is used as a target for an optical microscope having a magnification of 250×. This magnification is obtained by using 50× and 5× objective lenses. In this measurement, the through focuses of images are obtained from a CCD detector. Then, the focus-metric signature is calculated from the images. Finally, the focus-metric signatures of the simulation and the measurement are compared. From the comparison, it is shown that a nanoscale resolution can be achieved in the through-focus focus-metric method when the two-pitch grating target is used.

References

[1] J.W. Goodman, Introduction to Fourier Optics, McGraw-Hill, New York, 1996.
[2] H.E. Hwang, G.H. Yang, J.C. Chou, Opt. Eng. 41 (2002) 2620.
[3] S. Bushman, S. Farrer, Proc. SPIE 3213 (1997) 79.
[4] H.T. Huang, G. Raghavendra, A. Sezginer, K. Johnson, Proc. SPIE 5038 (2003) 126.
[5] W. Yang, L.W. Roger, S. Rabello, Proc. SPIE 5038 (2003) 200.
[6] N. Chateau, J.P. Hugonin, J. Opt. Soc. Am. A 11 (1994) 1321.
[7] M.G. Moharam, E.B. Grann, D.A. Pommet, J. Opt. Soc. Am. A 12 (1995) 1068.
[8] E.N. Glytsis, T.K. Gaylord, J. Opt. Soc. Am. A 4 (1987) 2061.
[9] Y.S. Ku, A.S. Liu, N. Smith, Opt. Express 13 (2005) 6699.
[10] R.M. Silver, R. Attota, M. Stocker, M. Bishop, J. Jun, R. Larrabee, Proc. SPIE 5752 (2005) 67.
[11] R. Attota, R.M. Silver, T.A. Germer, M. Bishop, Proc. SPIE 5752 (2005) 1441.
[12] M. Subbarao, J.K. Tyan, IEEE Trans. Pattern Anal. Mach. Intell. 20 (1998) 864.
[13] J.S. Ye, B.Z. Dong, B.Y. Gu, G.Z. Yang, S.T. Liu, J. Opt. Soc. Am. A 19 (2002) 2030.
[14] J.S. Ye, B.Y. Gu, B.Z. Dong, S.T. Liu, J. Opt. Soc. Am. A 22 (2005) 862.
[15] K. Hirayama, E.N. Glytsis, T.K. Gaylord, J. Opt. Soc. Am. A 14 (1997) 907.
[16] Y. Nakata, M. Koshiba, J. Opt. Soc. Am. A 7 (1990) 1494.
[17] J.E. Akin, Application and Implementation of Finite Element Methods, Academic, London, 1982.
[18] A. Taflove, Finite-Difference Time-Domain Method, Artech House, Boston, 1995.
[19] R. Harrington, Time-Harmonic Electromagnetic Fields, McGraw-Hill, New York, 1961.
[20] K. Hirayama, K. Igarashi, Y. Hayashi, J. Opt. Soc. Am. A 16 (1999) 1294.
[21] D.M. Shyu, M.H. Lu, Rev. Sci. Instr. 77 (2006).
[22] H.F. Talbot, Philos. Mag. 9 (1836).